Pergamon

Int. J. Mech. Sci. Vol. 38, No. 12, pp. 1285–1293, 1996

0020-7403/96 $15.00 + 0.00

PII:S0020-7403(96)00002-1

IN-PLANE RESPONSE OF A ROTATING ANNULAR DISK UNDER FIXED CONCENTRATED EDGE LOADS

JEN-SAN CHEN and JHI-LU JHU

Department of Mechanical Engineering, National Taiwan University, Taipei, Taiwan 107, Republic of China

(*Received* 27 *July* 1995)

Abstract—This paper investigates the in-plane response of a rotating annular disk under concentrated edge loads with both the radial and tangential components. Lame's potentials are used to simplify the highly coupled equilibrium equations. It is demonstrated that the problem of fixed disk–rotating load differs from the problem of rotating disk–fixed load not only by the centrifugal effect, but also by additional terms arising from Coriolis effect. While the effect of these Coriolis terms may be negligible when the rotational speed is small or the concentrated edge load is in the radial direction, they are important in the high rotational speed range when the concentrated edge load is in the tangential direction. Numerical results of the natural frequencies and steady-state response are presented for a radius ratio of 0.3 with emphasis on the difference between the responses of fixed disk–rotating load and rotating disk–fixed load systems. Copyright © 1996 Elsevier Science Ltd.

Keywords: in-plane response, rotating disk, Lame's potential.

NOMENCLATURE

a, b	inner and outer radii of the annular disk
c_n, d_n, e_n, f_n	constants of homogeneous solution
A_n, B_n	constants of particular solution
E	Young's modulus
G, H	functions used in the equilibrium equations
$L_{11}, L_{12}, L_{21}, L_{22}$	differential operators
r^*, η	polar coordinates with respect to the inertial frame
r	dimensionless coordinate in radial direction
$s_{n1}, s_{n2}, \beta_{n1}, \beta_{n2}$	parameters used in solving the general solution
t^*	time
t	dimensionless time
u_r^*, u_η^*	in-plane displacements
u_r, u_η	dimensionless in-plane displacements
β	distribution angle of edge traction
ρ	mass density
ν	Poisson's ratio
ζ	radius ratio
λ_1, λ_2	constants depending on Poisson's ratio
ϕ, ψ	Lame's potentials
$\sigma_{rr}^*, \sigma_{r\eta}^*$	stresses
$\sigma_{rr}, \sigma_{r\eta}$	dimensionless stresses
ω_{mn}	dimensionless natural frequency
Φ_{mn}, Ψ_{mn}	separable solutions used in calculating natural frequencies
$\Phi_{nc}, \Phi_{ns}, \Psi_{nc}, \Psi_{ns}$	separable solutions used in calculating steady-state response
Ω^*	rotational speed
Ω	dimensionless rotational speed

INTRODUCTION

It is well known that the natural frequencies of the in-plane radial and torsional vibrations of a spinning disk depend on the rotational speed. Bhuta and Jones [1] investigated the axisymmetric planar vibration of a rotating disk and found that the effect of rotation is generally to lower the natural frequencies. The same problem was studied by Doby [2] with different formulation. Burdess *et al.* [3] generalized the analysis to asymmetric in-plane vibration, and discussed the properties of both the forward and backward traveling circumferential waves.

The in-plane stress distribution in a fixed annular disk under fixed edge traction can be readily calculated by using the Airy stress function [4]. On the other hand, the investigations on the problem of a spinning disk under fixed edge loads are relatively rare, partly due to the complex Coriolis coupling associated with the relative motion between the rotating disk and the non-rotating loads. In practice, this study may find application in such fields as wood cutting industry or grinding wheel operation. In order to avoid the difficulties imposed by the Coriolis terms and the in-plane stresses due to centrifugal effect, Srinivasan and Ramamurti [5] investigated a relevant problem of a fixed disk under rotating concentrated edge loads with both radial and tangential components. While their investigation sheds some light on the dynamic effect of rotating loads on the fixed disk, the more important problem of a rotating disk under fixed concentrated edge load remains unsolved.

In the present paper we examine the in-plane stress distribution in a rotating disk under fixed concentrated edge loads. Both radial and tangential edge loads are considered. Instead of using a delta function to represent the concentrated load, we consider the edge load as a smoothly varying distributed traction over a narrow region of the outer boundary. Faster convergence is demonstrated with this arrangement. The equations of in-plane vibration of the rotating disk with respect to the inertial frame are first derived. Lame's potentials are used to simplify the highly coupled equations. Numerical results of the natural frequencies and steady-state response are presented for a radius ratio of 0.3 with emphasis on the difference between the responses of fixed disk–rotating load and rotating disk–fixed load systems.

EQUATIONS OF MOTION

Figure 1 shows an annular disk rotating at constant speed Ω^*. The material of the disk is assumed to be homogeneous and isotropic with mass density ρ, Young's modulus E and Poisson's ratio ν. The rotating disk is clamped at the inner radius $r^* = a$, and is subject to non-rotating edge tractions $\hat{\sigma}_{rr}^*$ and $\hat{\sigma}_{r\eta}^*$ at the outer radius $r^* = b$. (r^*, η) are the polar coordinates of a point in the rotating disk with respect to an inertial frame. If the disk is thin, plane stress conditions can be assumed and the in-plane displacements in the radial and tangential directions are denoted as u_r^* and u_η^*, respectively.

It is convenient to introduce some dimensionless variables,

$$r = \frac{r^*}{b}, \quad \zeta = \frac{a}{b}, \quad u_r = \frac{u_r^*}{b}, \quad u_\eta = \frac{u_\eta^*}{b}, \quad \Omega = \Omega^* b \sqrt{\frac{\rho}{E}},$$

$$t = \frac{t^*}{b}\sqrt{\frac{E}{\rho}}, \quad \sigma_{rr} = \frac{\sigma_{rr}^*}{E}, \quad \sigma_{r\eta} = \frac{\sigma_{r\eta}^*}{E}$$

where t^* represents the physical time. The equations of motion in terms of the dimensionless variables defined above with respect to the inertial frame can be written as follows [6],

$$\frac{1}{(1-\nu^2)}(L_{11}u_r + L_{12}u_\eta) = \left(\frac{\partial^2 u_r}{\partial t^2} + 2\Omega\frac{\partial^2 u_r}{\partial t\,\partial\eta} + \Omega^2\frac{\partial^2 u_r}{\partial\eta^2}\right) - 2\Omega\left(\frac{\partial u_\eta}{\partial t} + \Omega\frac{\partial u_\eta}{\partial\eta}\right) - \Omega^2(u_r + r) \quad (1)$$

$$\frac{1}{(1-\nu^2)}(L_{21}u_r + L_{22}u_\eta) = \left(\frac{\partial^2 u_\eta}{\partial t^2} + 2\Omega\frac{\partial^2 u_\eta}{\partial t\,\partial\eta} + \Omega^2\frac{\partial^2 u_\eta}{\partial\eta^2}\right) + 2\Omega\left(\frac{\partial u_r}{\partial t} + \Omega\frac{\partial u_r}{\partial\eta}\right) - \Omega^2 u_\eta \quad (2)$$

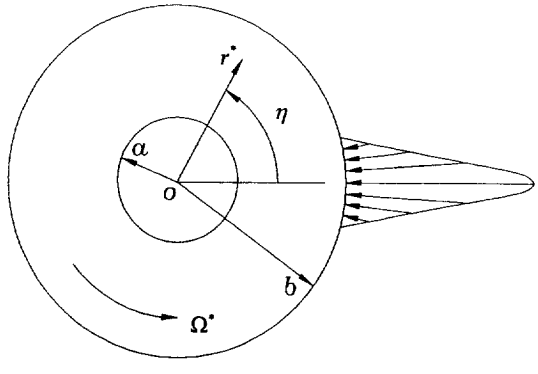

Fig. 1. A spinning annular disk under space-fixed edge load.

where the differential operators L_{11}, L_{12}, L_{21} and L_{22} are defined as

$$L_{11} = \frac{\partial^2}{\partial r^2} + \frac{1}{r}\frac{\partial}{\partial r} - \frac{1}{r^2} + \frac{1-\nu}{2r^2}\frac{\partial^2}{\partial \eta^2} \tag{3}$$

$$L_{12} = \frac{1+\nu}{2}\frac{1}{r}\frac{\partial^2}{\partial r\,\partial \eta} - \frac{3-\nu}{2}\frac{1}{r^2}\frac{\partial}{\partial \eta} \tag{4}$$

$$L_{21} = \frac{1+\nu}{2}\frac{1}{r}\frac{\partial^2}{\partial r\,\partial \eta} + \frac{3-\nu}{2}\frac{1}{r^2}\frac{\partial}{\partial \eta} \tag{5}$$

$$L_{22} = \frac{1-\nu}{2}\left(\frac{\partial^2}{\partial r^2} + \frac{1}{r}\frac{\partial}{\partial r} - \frac{1}{r^2}\right) + \frac{1}{r^2}\frac{\partial^2}{\partial \eta^2}. \tag{6}$$

The dimensionless boundary conditions with respect to the inertial frame are

$$u_r = u_\eta = 0 \quad \text{at } r = \zeta \tag{7}$$

$$\begin{aligned} &\frac{1}{1-\nu^2}\left[\frac{\partial u_r}{\partial r} + \nu\left(\frac{u_r}{r} + \frac{1}{r}\frac{\partial u_\eta}{\partial \eta}\right)\right] = \hat{\sigma}_{rr}(\eta) \\ &\qquad\qquad \text{at } r = 1. \\ &\frac{1}{2(1+\nu)}\left(\frac{1}{r}\frac{\partial u_r}{\partial \eta} + \frac{\partial u_\eta}{\partial r} - \frac{u_\eta}{r}\right) = \hat{\sigma}_{r\eta}(\eta) \end{aligned} \tag{8}$$

Another problem relevant to the above is a fixed disk subjected to edge traction rotating with constant speed Ω [5]. For this problem the dimensionless equations of motion with respect to a frame rotating with the edge traction can be written as

$$\frac{1}{(1-\nu^2)}(L_{11}u_r + L_{12}u_\eta) = \frac{\partial^2 u_r}{\partial t^2} + 2\Omega\frac{\partial^2 u_r}{\partial t\,\partial \eta} + \Omega^2\frac{\partial^2 u_r}{\partial \eta^2} \tag{9}$$

$$\frac{1}{(1-\nu^2)}(L_{21}u_r + L_{22}u_\eta) = \frac{\partial^2 u_\eta}{\partial t^2} + 2\Omega\frac{\partial^2 u_\eta}{\partial t\,\partial \eta} + \Omega^2\frac{\partial^2 u_\eta}{\partial \eta^2}. \tag{10}$$

The associated boundary conditions are in the same form as in Eqns (7) and (8). It should be understood that the coordinates (r, η) in Eqns (9) and (10) and the boundary conditions are associated with the rotating frame. By comparing Eqns (1, 2) with Eqns (9) and (10) we can see that the rotating disk–fixed load problem differs from the fixed disk–rotating load problem, mathematically, not only by the centrifugal effect but also by the additional terms arising from Coriolis coupling. While it is well known that the centrifugal effect will cause axisymmetrical stress field in the rotating disk, it is not clear how the Coriolis terms affect the steady-state stress distribution in a rotating disk under fixed edge traction. In other words, it is not clear how close the solutions of the fixed disk–rotating load system approximate the solutions of the rotating disk–fixed load system besides the stresses due to centrifugal effect.

NATURAL FREQUENCIES

Before calculating the steady state stress distribution, we first consider the natural frequencies of the freely rotating disk with respect to the inertial frame. It is noted that the differential equation (1) is inhomogeneous due to the body force term $r\Omega^2$. As the disk rotates at a certain speed, steady-state in-plane displacements $u_r^{(s)}(r, \eta)$ and $u_\eta^{(s)}(r, \eta)$ are induced due to the centrifugal effect. We consider small perturbations in displacements, $\hat{u}_r(r, \eta; t)$ and $\hat{u}_\eta(r, \eta; t)$, superposed on the steady-state solutions. By substituting the total displacements, $u_r^{(s)} + \hat{u}_r$ and $u_\eta^{(s)} + \hat{u}_\eta$, into the equilibrium equations (1) and (2), we can obtain the equations of vibration in terms of small displacement perturbations $\hat{u}_r$ and $\hat{u}_\eta$. The resulted equations are similar to Eqns (1) and (2) with $r\Omega^2$ in Eqn (1) being deleted and displacements u_r and u_η being replaced by $\hat{u}_r$ and $\hat{u}_\eta$, respectively. In the following discussion on natural frequencies we neglect the superposed hats on $\hat{u}_r$ and $\hat{u}_\eta$ for brevity. The boundary conditions for the freely rotating disk are similar to Eqns (7) and (8) with $\hat{\sigma}_{rr}(\eta) = \hat{\sigma}_{r\eta}(\eta) = 0$.

Equations (1) and (2) can be simplified if Lame's potentials ϕ and ψ are introduced [7]

$$u_r = \frac{\partial \varphi}{\partial r} + \frac{1}{r}\frac{\partial \psi}{\partial \eta} \tag{11}$$

$$u_\eta = \frac{1}{r}\frac{\partial \phi}{\partial \eta} - \frac{\partial \psi}{\partial r}. \tag{12}$$

Substituting Eqns (11) and (12) into the homogeneous parts of Eqns (1) and (2) results in the following equations

$$\frac{\partial G}{\partial r} + \frac{1}{r}\frac{\partial H}{\partial \eta} = 0 \tag{13}$$

$$\frac{1}{r}\frac{\partial G}{\partial \eta} - \frac{\partial H}{\partial r} = 0 \tag{14}$$

where

$$G = \lambda_1^2 \nabla^2 \phi - \Omega^2 \frac{\partial^2 \phi}{\partial \eta^2} + \Omega^2 \phi - 2\Omega^2 \frac{\partial \psi}{\partial \eta} - \frac{\partial^2 \phi}{\partial t^2} - 2\Omega \frac{\partial^2 \phi}{\partial t\, \partial \eta} - 2\Omega \frac{\partial \psi}{\partial t} \tag{15}$$

$$H = \lambda_2^2 \nabla^2 \psi - \Omega^2 \frac{\partial^2 \psi}{\partial \eta^2} + \Omega^2 \psi + 2\Omega^2 \frac{\partial \phi}{\partial \eta} - \frac{\partial^2 \psi}{\partial t^2} - 2\Omega \frac{\partial^2 \psi}{\partial t\, \partial \eta} + 2\Omega \frac{\partial \phi}{\partial t}. \tag{16}$$

λ_1 and λ_2 are two constants depending on the Poisson ratio,

$$\lambda_1^2 = \frac{1}{1 - \nu^2}, \quad \lambda_2^2 = \frac{1}{2(1 + \nu)}. \tag{17}$$

Equations (15) and (16) are two inhomogeneous equations for ϕ and ψ. The complete solutions of ϕ and ψ include time-independent particular solutions and time-dependent homogeneous solutions. While the particular solutions are important in determining the steady-state response as will be discussed later, they have nothing to do with the natural frequencies of the system. On the other hand, the homogeneous solutions of ϕ and ψ (with $G = H = 0$) are assumed to be in the following separable forms,

$$\phi(r, \eta; t) = \Phi_{mn}(r) e^{in\eta} e^{-i\omega_{mn} t} \tag{18}$$

$$\psi(r, \eta; t) = -i\Psi_{mn}(r) e^{in\eta} e^{-i\omega_{mn} t} \tag{19}$$

where

$$\Phi_{mn}(r) = c_n J_n(\beta_{n1} r) + d_n s_{n1} J_n(\beta_{n2} r) + e_n Y_n(\beta_{n1} r) + f_n s_{n1} Y_n(\beta_{n2} r) \tag{20}$$

$$\Psi_{mn}(r) = c_n s_{n2} J_n(\beta_{n1} r) + d_n J_n(\beta_{n2} r) + e_n s_{n2} Y_n(\beta_{n1} r) + f_n Y_n(\beta_{n2} r). \tag{21}$$

J and Y are Bessel functions of the first and the second kinds. ω_{mn} represents the natural frequency of the rotating disk. s_{n1} and s_{n2} are defined as

$$s_{n1} = \frac{-2\Omega(\omega_{mn} - n\Omega)}{(\omega - n\Omega)^2 + \Omega^2 + \lambda_1^2 \beta_{n2}^2} \quad \text{and} \quad s_{n2} = \frac{-2\Omega(\omega_{mn} - n\Omega)}{(\omega - n\Omega)^2 + \Omega^2 - \lambda_2^2 \beta_{n1}^2} \tag{22}$$

where β_{n1} and β_{n2} are positive real roots of the following quartic equation

$$\lambda_1^2 \lambda_2^2 \beta_n^4 - (\lambda_1^2 + \lambda_2^2)\beta_n^2 [(\omega_{mn} - n\Omega)^2 + \Omega^2] + [(\omega_{mn} - n\Omega)^2 + \Omega^2]^2 = 0. \tag{23}$$

After applying the homogeneous boundary conditions, we obtain four homogeneous algebraic equations with four unknowns c_n, d_n, e_n and f_n. For the existence of nontrivial solutions, the determinant of the coefficient matrix should vanish, and the frequency equation is then derived. For each n, which represents the number of nodal diameters, there is an infinite number of discrete ω_{mn} satisfying the frequency equation.

The solid lines in Fig. 2 represent the dimensionless natural frequency ω_{mn} as a function of the dimensionless rotational speed Ω for radius ratio $\zeta = 0.3$. For simplicity, only the modes with less than four nodal diameters are shown in Fig. 2. The Poisson ratio is assumed to be 0.3. The mode

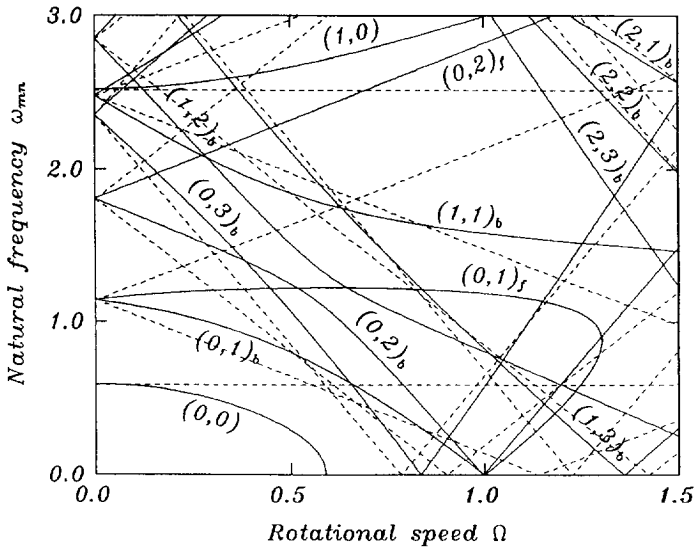

Fig. 2. The solid lines represent the natural frequencies of in-plane vibration of a freely rotating disk with respect to an inertial frame. The dashed lines represent the natural frequencies of a fixed disk as viewed by an observer rotating with speed Ω. The radius ratio of the disk is 0.3.

label $(m, n)_f$ represents the forward traveling modes with m nodal circles and n nodal diameters. Similarly, the subscript "b" represents a backward traveling wave. The critical speed Ω_{cn} is defined as the rotational speed at which the natural frequency of the mode $(0, n)_b$ vanishes. The first critical speed in Fig. 2 is $\Omega_{c0} = 0.591$ corresponding to the mode (0, 0). Beyond this critical speed the natural frequency ω_{00} becomes purely imaginary, and divergence instability is induced. It is noted that mode (0, 0) is a torsional mode which involves displacement u_η only, while mode (1, 0) is a radial mode which involves displacement u_r only [6]. All the modes with nodal diameters involve both torsional and radial vibrations at the same time.

The natural frequencies of a fixed disk as viewed by a rotating observer are much easier to obtain. First of all the natural frequencies ω_{mn} of the fixed disk as viewed by a non-rotating observer have been discussed in [5]. To a rotating observer, each of these natural frequencies splits into two, i.e. $\omega_{mn} + n\Omega$ and $\omega_{mn} - n\Omega$, except the axisymmetrical modes (i.e. $n = 0$) whose natural frequencies appear the same to both the fixed and the rotating observers. The dashed lines in Fig. 2 represent the natural frequencies of the fixed disk as viewed by an observer rotating with speed Ω.

The natural frequency loci in Fig. 2 offer valuable insight into the steady-state response of the disk under edge load. For a rotating disk under fixed edge traction with distribution $\cos n\eta$, its response tends to grow unboundedly as its rotational speed approaches the critical speed Ω_{cn}. These physical interpretations will be helpful in understanding the steady-state response of a rotating disk under concentrated edge load.

STEADY-STATE RESPONSE

In calculating the steady-state response of the rotating disk we assume that the edge traction is applied for a long time and the steady-state prevails as seen by an observer in the inertial frame. It is noted that both the differential Eqns (1) and (2), and the boundary conditions (7) and (8) are inhomogeneous. The superposition principle [8] permits us to decompose the problem into two simpler parts; one with inhomogeneous equations and homogeneous boundary conditions, and the other with homogeneous equations and inhomogeneous boundary conditions. The solution of the original problem can be obtained by reassembling these solutions of the simpler problems. For the first part, the forcing term $r\Omega^2$ in the inhomogeneous Eqn (1) is due to the centrifugal effect. When the steady-state solutions are concerned, this term is dominant compared to other contribution from the term $u_r\Omega^2$. Therefore, the solution of the first problem is the same as the classical problem of a freely rotating disk, and is well documented in the literature [9]. On the other hand, the

second problem with homogeneous equations and inhomogeneous boundary conditions is rarely investigated and will be the subject of the following discussions.

The homogeneous parts of Eqns (1) and (2) are equivalent to Eqns (13) and (14), as explained in preceding section. When steady-state response is concerned, all the temporal derivatives are neglected and Eqns (15) and (16) are replaced by

$$G = \lambda_1^2 \nabla^2 \phi - \Omega^2 \frac{\partial^2 \phi}{\partial \eta^2} + \Omega^2 \phi - 2\Omega^2 \frac{\partial \psi}{\partial \eta} \tag{24}$$

$$H = \lambda_2^2 \nabla^2 \psi - \Omega^2 \frac{\partial^2 \psi}{\partial \eta^2} + \Omega^2 \psi + 2\Omega^2 \frac{\partial \phi}{\partial \eta}. \tag{25}$$

The general solutions for G and H in Eqns (24) and (25) can be expressed in the form

$$G = A_0 + \sum_{n=1}^{\infty} [(A_n r^n + B_n r^{-n}) \cos n\eta + (A_n' r^n + B_n' r^{-n}) \sin n\eta] \tag{26}$$

$$H = A_0' + \sum_{n=1}^{\infty} [(A_n' r^n - B_n' r^{-n}) \cos n\eta + (-A_n r^n + B_n r^{-n}) \sin n\eta] \tag{27}$$

where A_n, B_n, A_n' and B_n' are undetermined constants. Equations (24) and (25) are two inhomogeneous equations for ϕ and ψ. Since the corresponding solutions must be periodic in η, the general solutions for ϕ and ψ can be expressed in Fourier series as

$$\phi(r, \eta) = \Phi_{0c} + \sum_{n=1}^{\infty} \Phi_{nc}(r) \cos n\eta + \Phi_{ns}(r) \sin n\eta \tag{28}$$

$$\psi(r, \eta) = \Psi_{0c} + \sum_{n=1}^{\infty} \Psi_{nc}(r) \cos n\eta + \Psi_{ns}(r) \sin n\eta. \tag{29}$$

Since the Fourier components are orthogonal, the solutions can be treated separately for different Fourier components.

Case n $\neq$ 1. The nontrivial solutions for this case are

$$\Phi_{nc} = c_n J_n(\beta_{n1} r) + d_n s_{n1} J_n(\beta_{n2} r) + e_n Y_n(\beta_{n1} r) + f_n s_{n1} Y_n(\beta_{n2} r) \tag{30}$$

$$\Psi_{ns} = c_n s_{n2} J_n(\beta_{n1} r) + d_n J_n(\beta_{n2} r) + e_n s_{n2} Y_n(\beta_{n1} r) + f_n Y_n(\beta_{n2} r) \tag{31}$$

$$\Phi_{ns} = c_n' J_n(\beta_{n1} r) + d_n' s_{n1} J_n(\beta_{n2} r) + e_n' Y_n(\beta_{n1} r) + f_n' s_{n1} Y_n(\beta_{n2} r) \tag{32}$$

$$\Psi_{nc} = -c_n' s_{n2} J_n(\beta_{n1} r) - d_n' J_n(\beta_{n2} r) - e_n' s_{n2} Y_n(\beta_{n1} r) - f_n' Y_n(\beta_{n2} r) \tag{33}$$

where $s_{n1}, s_{n2}, \beta_{n1}$, and β_{n2} are defined by Eqns (22) and (23) with ω_{mn} being specified to be zero.

Case n = 1. The solution for this case cannot be generalized from the case $n \neq 1$, because one of the two β's vanishes. The nontrivial solutions for this case can be found as

$$\Phi_{1c} = d_1 s_{11} J_1(\beta_{12} r) + f_1 s_{11} Y_1(\beta_{12} r) + A_1 \frac{r}{2\Omega^2} + B_1 \frac{r \ln r}{\lambda_1^2 + \lambda_2^2} \tag{34}$$

$$\Psi_{1s} = d_1 J_1(\beta_{12} r) + f_1 Y_1(\beta_{12} r) + B_1 \frac{1}{\lambda_1^2 + \lambda_2^2} \left(r \ln r + \frac{\lambda_1^2 - \lambda_2^2}{2r\Omega^2} \right) \tag{35}$$

$$\Phi_{1s} = d_1' s_{11} J_1(\beta_{12} r) + f_1' s_{11} Y_1(\beta_{12} r) + A_1' \frac{r}{2\Omega^2} + B_1' \frac{r \ln r}{\lambda_1^2 + \lambda_2^2} \tag{36}$$

$$\Psi_{1c} = -d_1' J_1(\beta_{12} r) - f_1' Y_1(\beta_{12} r) - B_1' \frac{1}{\lambda_1^2 + \lambda_2^2} \left(r \ln r + \frac{\lambda_1^2 - \lambda_2^2}{2r\Omega^2} \right) \tag{37}$$

where β_{12} and s_{11} are found to be

$$\beta_{12} = \frac{\sqrt{3 - \nu}}{\lambda_2} \Omega \quad \text{and} \quad s_{11} = -\frac{1 - \nu}{2}.$$

The constants c_n, d_n, e_n, f_n, A_n, B_n and their primed counterparts in Eqns (30–37) can be determined by the inhomogeneous boundary conditions.

For the steady-state response of a fixed disk under rotating edge load Eqns (13) and (14) should read

$$G = \lambda_1^2 \nabla^2 \phi - \Omega^2 \frac{\partial^2 \phi}{\partial \eta^2}, \quad H = \lambda_2^2 \nabla^2 \psi - \Omega^2 \frac{\partial^2 \psi}{\partial \eta^2}.$$

It is noted that the equilibrium equations for the fixed disk–rotating load system are decoupled into equations for ϕ and ψ, respectively, and the stress distribution as viewed by an observer rotating with speed Ω has beed examined in [5].

CONCENTRATED EDGE LOADS

We first assume that the normal edge traction $\hat{\sigma}_{rr}(\eta)$ distributes over a small range on the outer boundary from $\eta = -\beta$ to β in the following form

$$\hat{\sigma}_{rr}(\eta) = \frac{1}{2\beta}\left(1 + \cos\frac{\pi\eta}{\beta}\right) \quad \text{for } -\beta \leqslant \eta \leqslant \beta. \tag{38}$$

As β approaches zero, Eqn (38) may simulate a concentrated force with unit magnitude. Equation (38) can be expanded in the following Fourier series,

$$\hat{\sigma}_{rr}(\eta) = \frac{1}{2\pi} + \sum_{n=1}^{\infty} \frac{\pi \sin n\beta \cos n\eta}{n\beta(\pi^2 - n^2\beta^2)}. \tag{39}$$

From boundary condition (39) and $\hat{\sigma}_{r\eta}(\eta) = 0$, together with the zero displacement conditions (7) on the inner radius one can determine the constants in Eqns (30–37) uniquely. In the case when the edge load is in the tangential direction, the roles of $\hat{\sigma}_{rr}(\eta)$ and $\hat{\sigma}_{r\eta}(\eta)$ are exchanged.

Tables 1 and 2 show the results of a convergence test on the stresses for the cases of rotating disk–fixed load and fixed disk–rotating load, respectively. The columns labeled σ_{rr} and $\sigma_{r\eta}$ show the stresses at various radii when the edge tractions are in the radial and tangential directions, respectively. The radius ratio of the disk is 0.3, and the rotational speed $\Omega = 0.5$. The angle of edge traction distribution 2β is taken to be 10 degrees. As expected, the stresses converge faster when edge traction distribution (38) is assumed, as compared to the case of a delta function used in [5]. In the following calculations 50 terms are used in the summations (28) and (29).

Table 1. Convergence test for a rotating disk under fixed concentrated edge load. The radius ratio is 0.3, and the rotational speed $\Omega = 0.5$

	σ_{rr}		$\sigma_{r\eta}$	
Radius	50 terms	70 terms	50 terms	70 terms
0.3	1.9627007	1.9627007	7.1025632	7.1025632
0.5	2.4019989	2.4019989	2.3432113	2.3432113
0.7	3.9279871	3.9279940	0.5004403	0.5004349
0.9	10.6590257	10.7647320	− 1.7836641	− 1.8626198

Table 2. Convergence test for a fixed disk under rotating concentrated edge load. The radius ratio is 0.3, and the rotational speed $\Omega = 0.5$

	σ_{rr}		$\sigma_{r\eta}$	
Radius	50 terms	70 terms	50 terms	70 terms
0.3	2.2012810	2.2012810	2.7130206	2.7130206
0.5	2.6446471	2.6446471	0.8581873	0.8581873
0.7	4.0766234	4.0766303	0.0367004	0.0367057
0.9	10.6056926	10.7106894	− 1.7821996	− 1.8601687

Figures 3 and 4 show the stress distributions σ_{rr} and $\sigma_{r\eta}$, in the circumferential direction at the radius $r = 0.7$ when the concentrated edge loads are in the radial and tangential directions, respectively. All the stresses due to centrifugal effect are excluded in these figures. The solid lines represent the case of a disk rotating at $\Omega = 0.5$ and subjected to fixed edge load. The dashed lines represent the stress distribution in a fixed disk subjected to edge load rotating at $\Omega = 0.5$, as viewed by an observer rotating with the edge load. The dotted lines represent the case of a fixed disk under fixed load, which are obtained through the use of Airy stress function [4]. As Ω approaches zero, both the solid and the dashed lines approach the dotted lines. In the case when $\Omega = 0.5$ and the edge traction is in the radial direction, the stress distribution σ_{rr} of the fixed disk–rotating load system is close to that of the rotating disk–fixed load system, as shown in Fig. 3. In the case when the edge

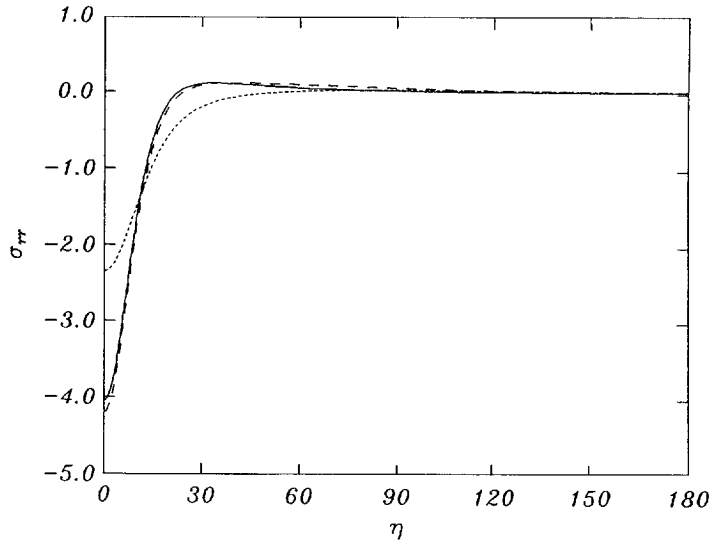

Fig. 3. The solid lines represent the stress distribution σ_{rr} along the circumferential direction at radius 0.7 for a disk rotating at $\Omega = 0.5$ under fixed normal edge traction in the form of Eqn (38). The dashed and the dotted lines represent the stress distributions for a fixed disk under rotating and fixed edge loads, respectively, with the same distribution.

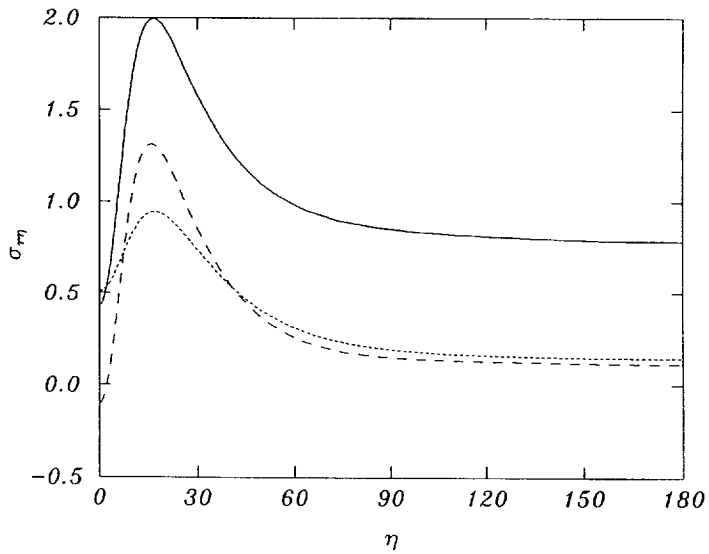

Fig. 4. The solid lines represent the stress distribution $\sigma_{r\eta}$ at radius 0.7 for a disk rotating at $\Omega = 0.5$ under fixed tangential edge traction in the form of Eqn (38). The dashed and the dotted lines represent the stress distributions for a fixed disk under rotating and fixed edge loads, respectively, with the same distribution.

load is in the tangential direction, on the other hand, Fig. 4 shows that the stress $\sigma_{r\eta}$ of the rotating disk–fixed load system is much larger than that of the fixed disk–rotating load system. In other words, the Coriolis terms in Eqns (1) and (2) have significant contributions when the rotating disk is under concentrated tangential load.

The response of the rotating disk under concentrated edge load can be considered as due to the combined effects of all the harmonics in Eqn (39). A careful inspection on the frequency loci in Fig. 2 reveals that the natural frequency of the mode (0, 0) of the rotating disk with respect to the inertial frame differs significantly from that of the fixed disk with respect to the rotating observer. In particular, when the rotating disk is under uniform tangential edge traction $\hat{\sigma}_{r\eta} = 1$, stress response in the disk will grow unboundedly when the rotational speed of the disk approaches Ω_{c0}. On the other hand, the stress field in the fixed disk under uniform edge load is independent of the rotational speed of the edge load. Based on the above examination, we conclude that the significant contribution of the Coriolis terms is primarily due to the axisymmetrical mode (0, 0), which is of torsional nature.

CONCLUSIONS

This paper investigates the natural frequencies of a freely rotating disk and the steady-state response of the rotating disk under fixed concentrated edge traction. Emphasis is given to the effect of the terms arising from Coriolis coupling. Another problem of a fixed disk under rotating edge traction is also presented for comparison. One of the obvious differences between these two problems is the stress field due to the centrifugal effect. On the other hand, the significance of the Coriolis terms are not so obvious and is the subject of this paper. The results of these studies can be summarized as follows.

(1) The apparent natural frequencies of a fixed disk as viewed by a rotating observer are linear functions of the rotational speed. In particular, the natural frequencies of the axisymmetrical modes are independent of the rotational speed. On the other hand, the natural frequencies of the rotating disk relative to the inertial frame are much more complex due to Coriolis coupling. Divergence instability is induced when the disk rotates beyond the critical speed Ω_{c0}.

(2) When the concentrated edge traction is in the tangential direction, it is found that the steady-state stress response of the rotating disk–fixed load system grows unboundedly as the rotational speed approaches the critical speed Ω_{c0}. On the other hand, the stresses of the fixed disk–rotating load system change only slightly compared to those of the rotating disk–fixed load problem.

(3) When the concentrated edge load is in the radial direction, the difference between the steady state responses of the rotating disk–fixed load system and the fixed disk–rotating load system is not as significant as the case with tangential load.

(4) The most significant harmonic component in the concentrated edge traction which causes the deviation between the stress distributions in the fixed disk–rotating load and the rotating disk–fixed load systems appears to be the axisymmetrical mode, which is of torsional nature.

REFERENCES

1. P. G. Bhuta and J. P. Jones, Symmetric planar vibrations of a rotating disc. *J. Acoust. Soc. Am.* **35**(7), 982–989 (1963).
2. R. Doby, On the elastic stability of Coriolis-coupled oscillations of a rotating disc. *Franklin Inst.* **288**(3), 203–212 (1969).
3. J. S. Burdess, T. Wren and J. N. Fawcett, Plane stress vibrations in rotating discs. *Proc. Instn Mech. Engrs* **201**, 37–44 (1987).
4. E. G. Coker and L. N. G. Filon, *A Treatise on Photo-Elasticity*. Cambridge University Press, London (1957).
5. V. Srinivasan and V. Ramamurti, Dynamic response of an annular disk to a moving concentrated, in-plane edge load. *J. Sound Vibration* **72**(2), 251–262 (1980).
6. J.-L. Jhu, In-plane stress and displacement distributions in a spinning annular disk under stationary edge loads, Master Thesis, Department of Mechanical Engineering, National Taiwan University (1995).
7. A. C. Eringen and W. S. Suhubi, *Elastodynamics*, Vol. II. Academic Press, New York (1975).
8. Ivar Stakgold, *Green's Function and Boundary Value Problems*. John Wiley & Sons, New York (1979).
9. K. Ono, J.-S. Chen and D. B. Bogy, Stability analysis of the head–disk interface in a flexible disk drive. *ASME J. Appl. Mech.* **58**(4), 1005–1014 (1991).